

Electronic Supplementary Information for

Improving the Stability and Selectivity for the Oxygen-Evolution Reaction on Semiconducting WO₃ Photoelectrodes with a Solid-State FeOOH Catalyst

Charles R. Lhermitte,^a J. Garret Verwer^a and Bart M. Bartlett^{a*}

Department of Chemistry, University of Michigan, 930 N. University Avenue, Ann Arbor, MI 48109-1055, United States

Email: bartmb@umich.edu

Table of Contents

Fig. S1. Powder XRD pattern of WO ₃ and WO ₃ -FeOOH	S2
Fig. S2. CL-LSV of WO ₃ after soaking in pH 4 and 7 KPi	S2
Fig. S3. SEM image of a cracked FeOOH	S3
Fig. S4. Powder XRD pattern of FeOOH grown on and FTO substrate	S3
Fig. S5. EDX spectrum of a WO ₃ -FeOOH electrode	S4
Fig. S6. F(R) spectrum for FeOOH Grown on FTO	S4
Fig. S7. CL-LSV of FeOOH grown on an FTO substrate	S4
Fig. S8. CL-LSVs of WO ₃ -FeOOH and WO ₃ under front and back illumination	S5
Fig. S9. O ₂ measurements under illumination for three WO ₃ -FeOOH electrodes	S5
Fig. S10. O ₂ measurements under illumination for three WO ₃ electrodes	S6
Fig. S11. CL-LSVs of WO ₃ -FeOOH before/after soaking in pH4 and pH 7 KPi solutions	S6
Fig. S12. EQE at different light chopping frequencies for WO ₃ and WO ₃ -FeOOH	S6
Fig. S13. Cross-sectional and top-down SEM images of a WO ₃ -FeOOH electrode	S7
Fig. S14. Electrochemical H ₂ O ₂ detection on a WO ₃ electrode	S7
Fig. S15. Electrochemical measurement of the surface area of WO ₃ and WO ₃ -FeOOH film	S8
Fig. S16. (EQE WO ₃ -FeOOH) / (EQE WO ₃) ratio	S8

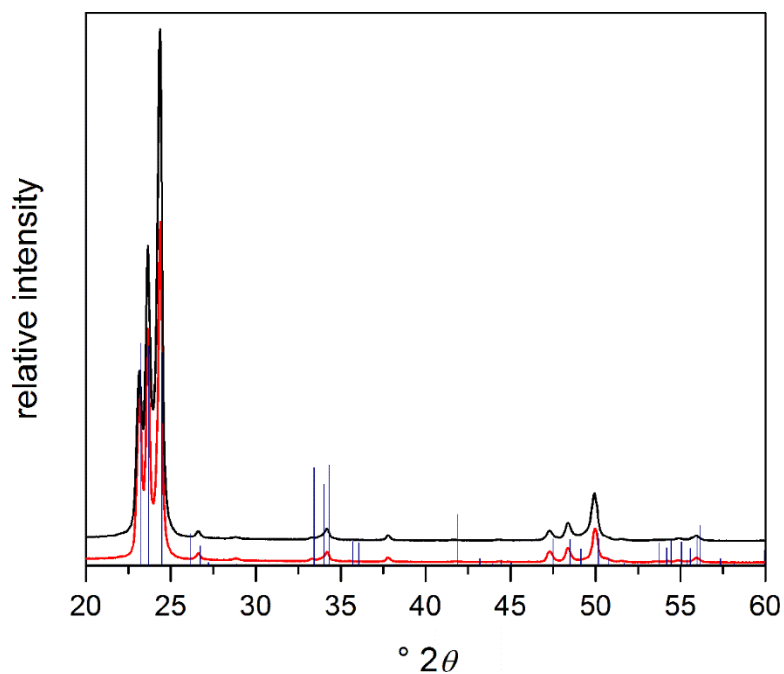


Fig. S1. Powder XRD pattern of WO_3 (black) and $\text{WO}_3\text{-FeOOH}$ (red). Blue vertical lines represent indexed Bragg reflections for monoclinic WO_3 .

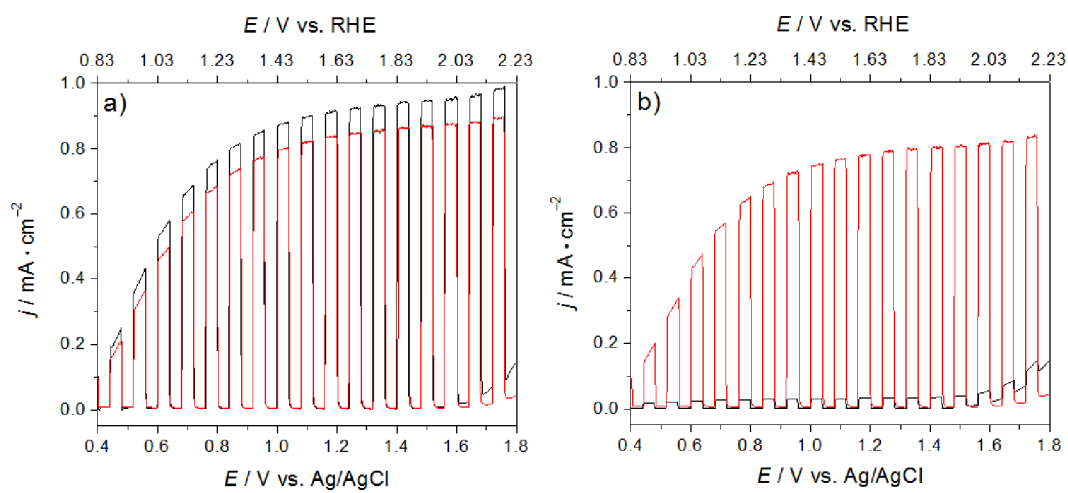


Fig. S2. CL-LSVs of WO_3 recorded before (red) and after (black) soaking 0.1 M KP_i buffer at a) pH 4; and b) pH 7.

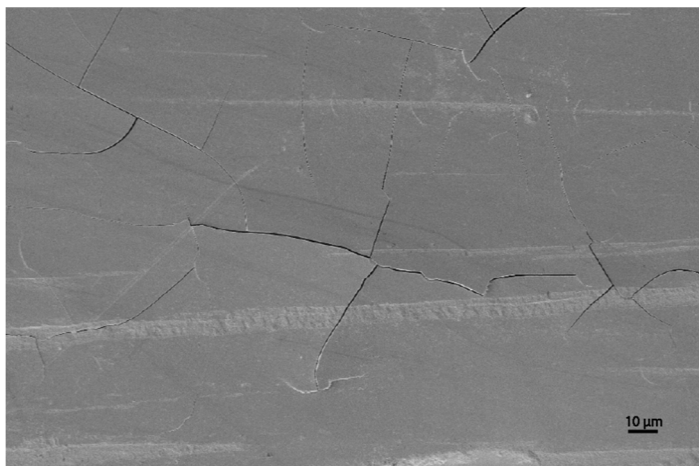


Fig. S3. SEM image of a cracked FeOOH on WO₃. The pictured film was synthesized using longer deposition times, generating a thicker layer. Cracking in the film was observed due to the film drying out.

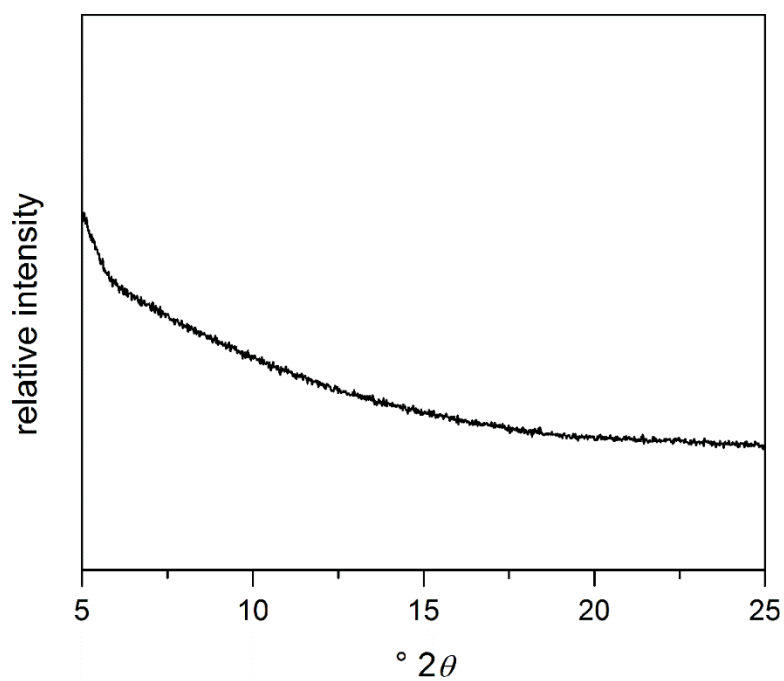


Fig. S4. Powder XRD pattern of FeOOH electrochemically deposited onto FTO showing no discernible Bragg reflections due to the amorphous nature of the film.

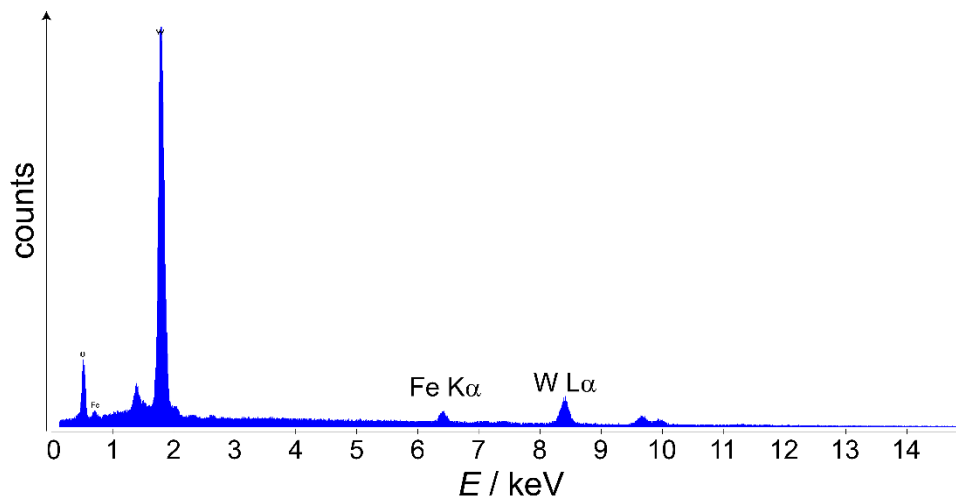


Fig. S5. EDX spectrum of a $\text{WO}_3\text{-FeOOH}$ electrode.

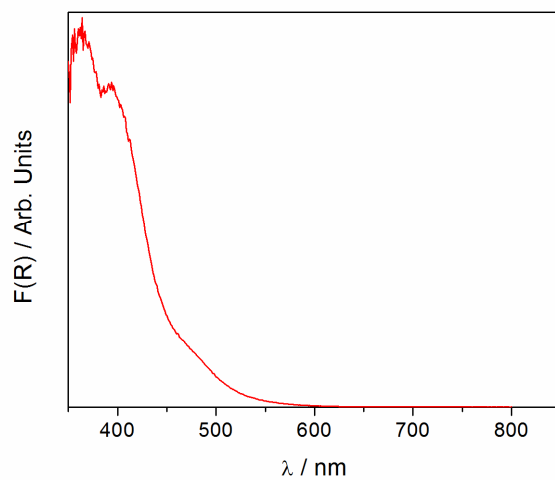


Fig. S6. F(R) spectrum for FeOOH electrochemically grown onto FTO.

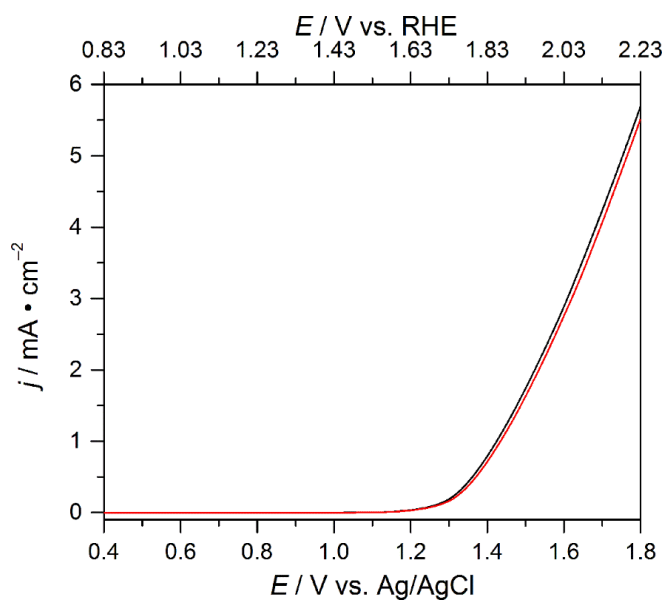


Fig. S7. LSV traces of FeOOH recorded in the dark (red) and under chopped light illumination (black).

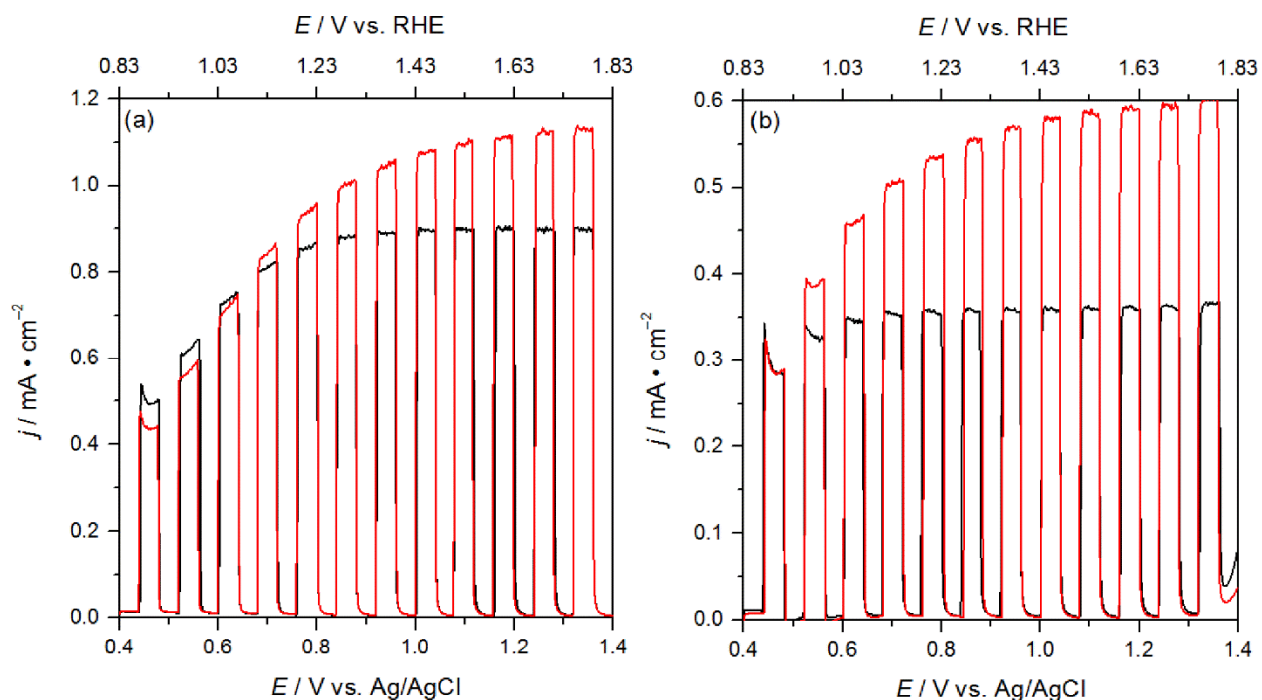


Fig. S8. CL-LSVs for a) WO_3 and b) FeOOH recorded in 0.1 M KP_i buffer at pH 4 under 100 mW/cm^2 AM1.5G illumination. The sweep rate is 20 mV/s. Data in black represent voltammograms recorded under front-side illumination, and data in red under back-side illumination.

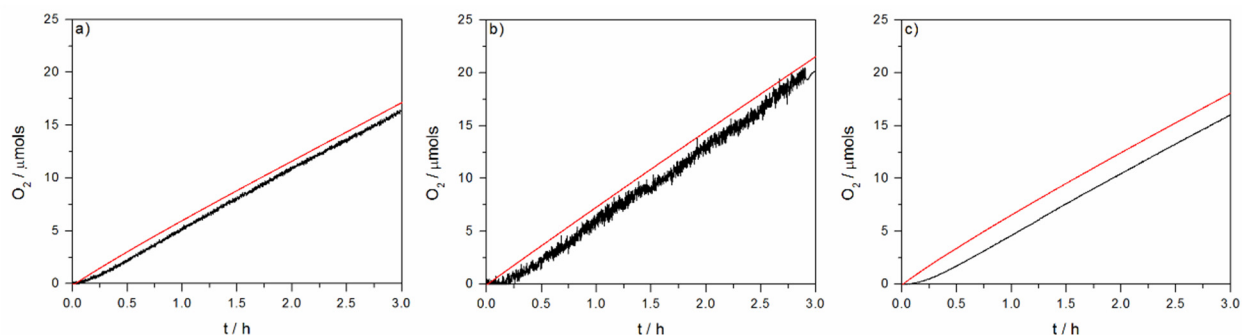


Fig. S9. Three trials of oxygen-evolution Faradaic efficiency measurements on $\text{WO}_3\text{-FeOOH}$ recorded at 1.43 V vs. RHE in 0.1 M KP_i buffer at pH 4 under 200 mW/cm^2 AM1.5G illumination. The red lines represent the theoretical yield of O_2 based on the charge passed, and the black lines indicate the O_2 measured by the Neofix O_2 fluorescence probe. For each experiment, a fresh $\text{WO}_3\text{-FeOOH}$ electrode was employed. From left to right, the Faradaic efficiencies are 95.6, 97.7, and 94.5% respectively.

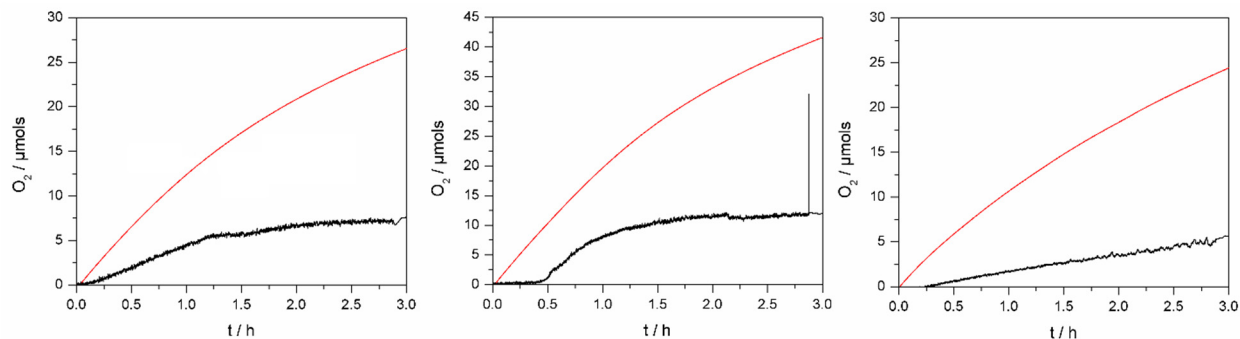


Fig. S10. Three trials of oxygen-evolution Faradaic efficiency measurements on WO₃ recorded at 1.43 V vs. RHE in 0.1 M KPi buffer at pH 4 under 200 mW/cm² AM1.5G illumination. The red lines represent the theoretical yield of O₂ based on the charge passed, and the black lines indicate the O₂ measured by the Neofix O₂ fluorescence probe. For each experiment, a fresh WO₃ electrode was employed. From left to right, the Faradaic efficiencies are 28.7, 28.8, and 23.1% respectively.

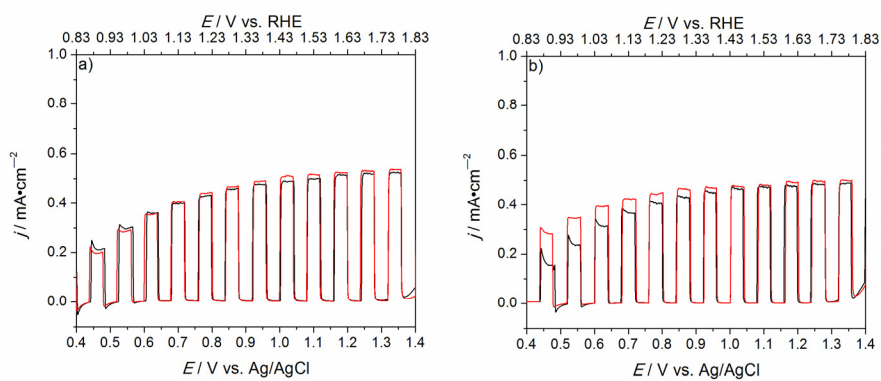


Fig. S11. CL-LSVs of a WO₃-FeOOH electrode before (black) and after (red) having been soaked overnight in a) 0.1M pH 4 KPi and b) 0.1M pH 7 KPi solutions. CL-LSVs were collected in 0.1M pH 4 KPi under 1 sun illumination at 20 mV/s.

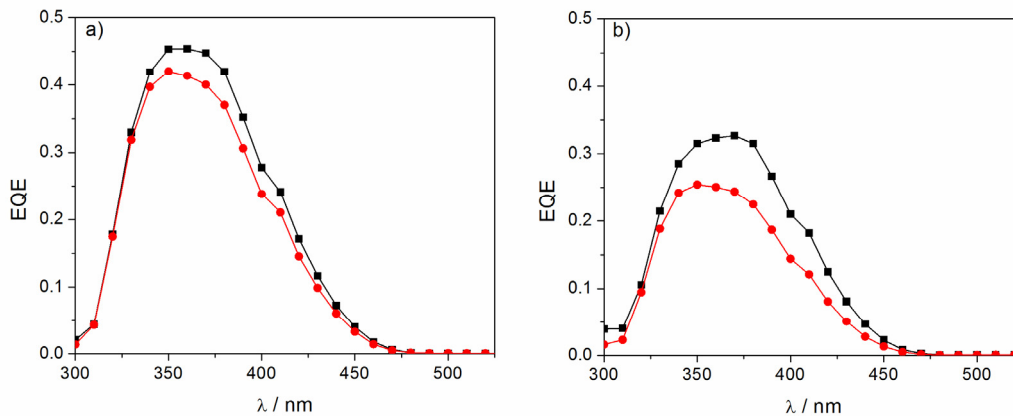


Fig. S12. EQE at different light chopping frequencies of a single WO₃ film before (a) and after (b) loading the FeOOH OEC. Black lines represent the EQE at 15Hz and red represent the EQE at 20 Hz.

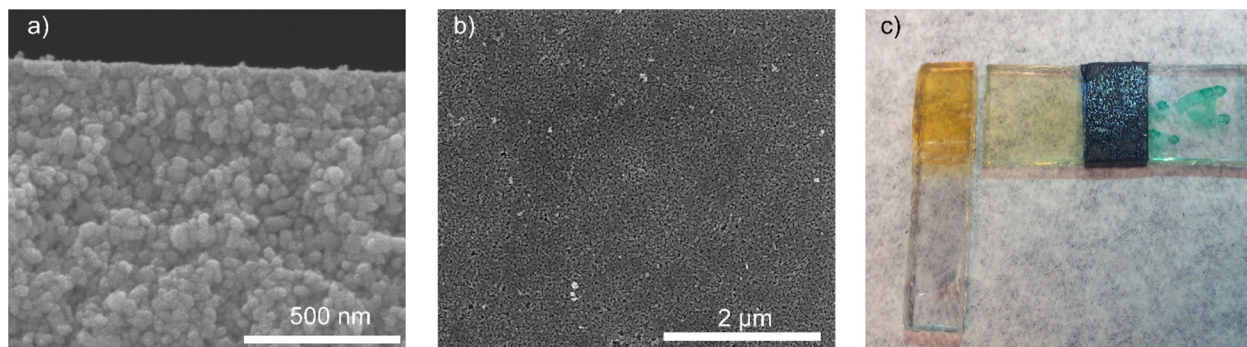


Fig. S13. 1) Cross-sectional SEM image of a $\text{WO}_3\text{-FeOOH}$ electrode; b) top-down SEM image, and c) photograph of the electrode. For c), the electrode on the left is the sample used for SEM imaging and the electrode on the right is a WO_3 film for comparison. No additional layer is visible in the cross-sectional SEM image, indicating that the FeOOH may grow primarily in the interstices of the film.

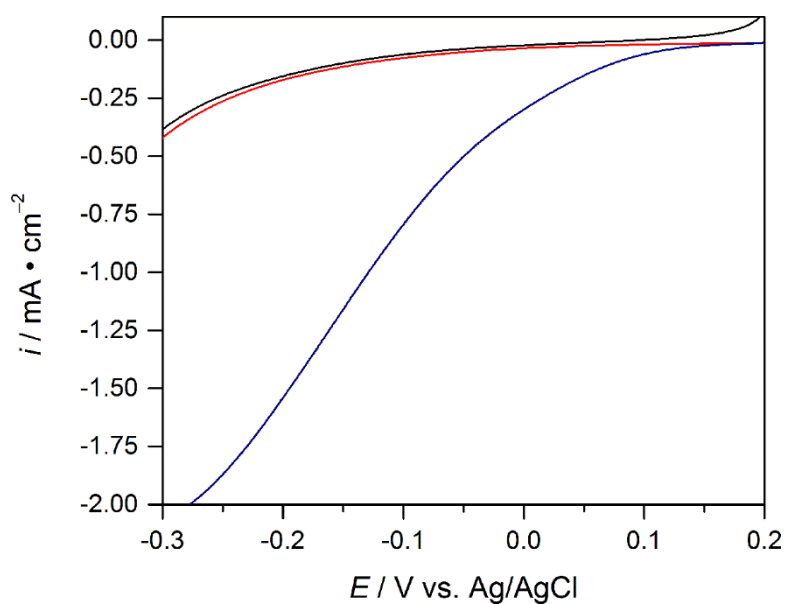


Fig. S14. Electrochemical detection of H_2O_2 on WO_3 . Cathodic LSV scans were recorded before (black) and after (red) CPC of a WO_3 electrode under 1-sun AM1.5G illumination at 1.23 V vs. RHE for 2 hours in a 0.1 M KPi buffer at pH 4. The blue line represents the cathodic scan of a WO_3 electrode in an identical solution that was spiked with 10 μL of H_2O_2 .

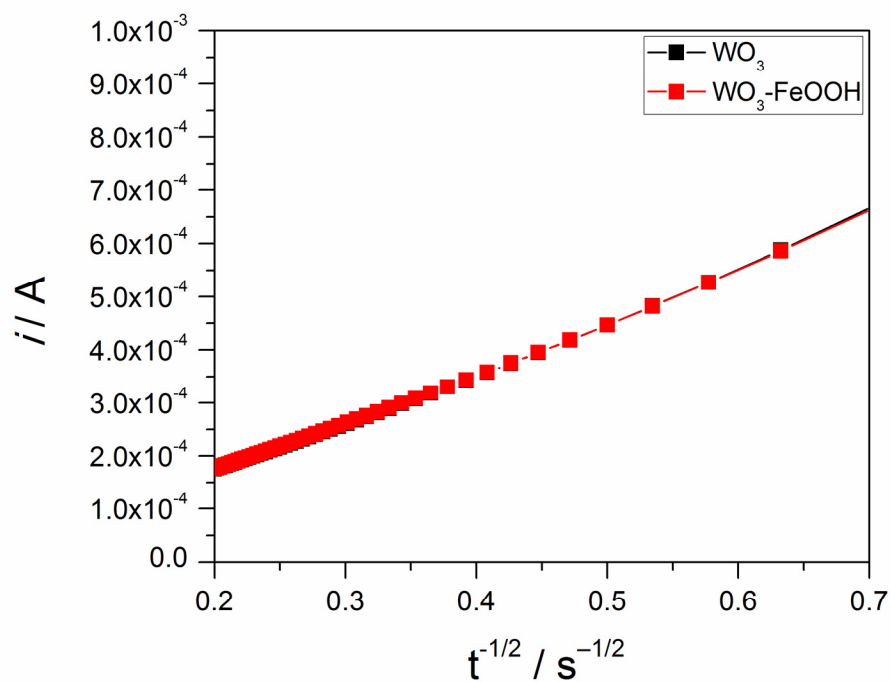


Fig. S15. Cottrell plot of the amperometric $i-t$ curve. $[Fe(CN)_6]^{3-}$ reduction was measured at -0.05 V vs. Ag/AgCl in a 0.1 M KCl solution containing 6 mM $K_3[Fe(CN)_6]$. The Cottrell equation predicts a linear change in i vs. $t^{-1/2}$ and the slope is proportional to the active surface area of the electrode.

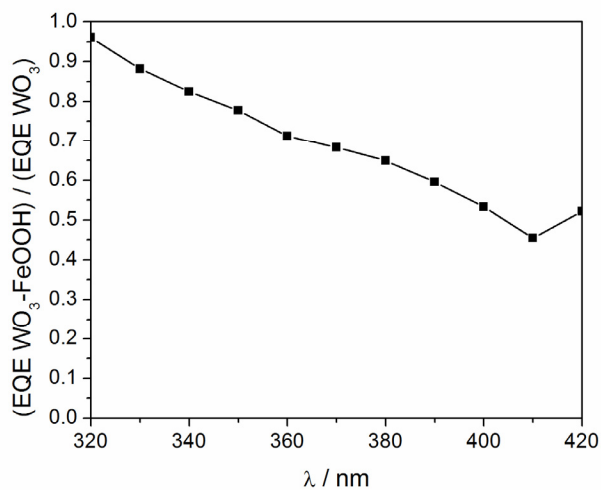


Fig. S16. $(EQE\ WO_3) / (EQE\ WO_3-FeOOH)$. This plot was constructed from the data represented in Fig. 7 of the manuscript by taking the EQE of $WO_3-FeOOH$ and dividing it by the EQE of WO_3 . A decrease in $(EQE\ WO_3-FeOOH) / (EQE\ WO_3)$ is observed with increasing λ due to parasitic absorption from the FeOOH.